Journal of Materials Chemistry C

ROYAL SOCIETY OF CHEMISTRY

PAPER

View Article Online
View Journal | View Issue

Cite this: J. Mater. Chem. C, 2024, 12, 7981

Significant chemiluminescence enhancement by tannic acid functionalised plasmonic silver nanoparticles†

Yao Lu, Jiamin Xu, D. Jason Riley and Fang Xie *

Received 15th March 2024,
Accepted 7th May 2024

DOI: 10.1039/d4tc01039f

rsc.li/materials-c

Chemiluminescence, a widely used optical method in forensic science and *in vitro* diagnosis, faces sensitivity limitations. This study introduces plasmonic enhanced chemiluminescence (PEC) using tannic acid-functionalised silver nanoparticles, achieving up to 175-fold increase in luminol chemiluminescence intensity. Systematic investigation deconvolutes key factors including nanoparticle size and surface functionalisation. A wider dynamic range and lower detection limit of Fe ions were demonstrated, even in anaemia situations. These findings advance ultrasensitive detection in chemiluminescence biosensors through PEC.

Introduction

Chemiluminescence is an interesting optical phenomenon which has a wide range of applications. Luminol, which emits blue light following a chemiluminescence reaction, was first used for analysing a crime scene in Germany.[1] Since then, blood detection at crime scenes has traditionally relied on the luminol–H_2O_2 chemiluminescence method, where the Fe ions in hemins act as catalysts to decompose the H_2O_2 and oxidise the luminol to produce luminescence.[2] Luminol is also widely applied in biological and chemical research as a substrate reagent for protein detection.[3]

Despite the achievements of fluorescence-based assays, certain inherent limitations, such as complex instrumentation, higher input costs, and susceptibility to background interference and photobleaching, have hindered universal accessibility and affordability.[4] Chemiluminescence on the other hand holds great promise as an attractive alternative to fluorescence-based biosensing. Chemiluminescence has the advantage that there is no need for an external light source and no unwanted background.[5,6] It has emerged as a promising technique in a wide range of applications due to its simplicity and relatively high signal output. Nonetheless, chemiluminescence faces significant limitations in trace detection, either in forensic science or biosensing, due to the low intensity of emitted light.[7]

Plasmonics is a recently established field that studies the interaction between light and metal nanostructures.[8] Although the foundation for describing the optical properties of metal nanoparticles was laid by Mie in 1908, plasmonics was not studied further until the significant breakthroughs in nanotechnology in the 1960s.[9] Incorporating plasmonic nanostructures to enhance fluorescence signals and elevate fluorescence-based biosensing has substantially bolstered sensitivity, leading to the development of exceptionally precise detection techniques.[10–13] In parallel, plasmonic nanoparticles were also incorporated into a chemiluminescent system, to form plasmonic enhanced chemiluminescence (PEC).[14]

Previous studies have proved the capability of Ag nanoparticles (NPs) to enhance luminol chemiluminescence. In one study, the silver nanoparticles act as a catalyst to accelerate the decomposition of H_2O_2 and form reactive intermediates, resulting in a stronger chemiluminescence signal.[15] In another test where chemiluminescence was conducted on a plasmonic Ag Island film, an enhancement of 20-fold in the chemiluminescence intensity was reported.[16] These findings strongly indicate that metal nanostructures can improve the signal-to-noise ratio to realise the application of chemiluminescence-based detection with higher sensitivity in both plasmonic and/or catalytic pathways.

Plasmonic and catalytic effects enhance luminol chemiluminescence differently. In the catalytic effect, the metal nanoparticles, such as Au or Ag, catalyse the decomposition of H_2O_2 and accelerate the reaction with luminol to emit light. It is well-studied that the catalytic effect increases with decreasing nanoparticle sizes.[15,17] In contrast, plasmonic nanoparticles utilise the localised surface plasmon resonance to couple with incident light and generate an enhanced electromagnetic field, leading to a stronger scattering and/or absorption.[12] However, the systematic study of the plasmonic effect in chemiluminescence is rarely investigated.

Materials Department, Imperial College London, London, SW7 2AZ, UK.
E-mail: f.xie@imperial.ac.uk

† Electronic supplementary information (ESI) available. See DOI: https://doi.org/10.1039/d4tc01039f

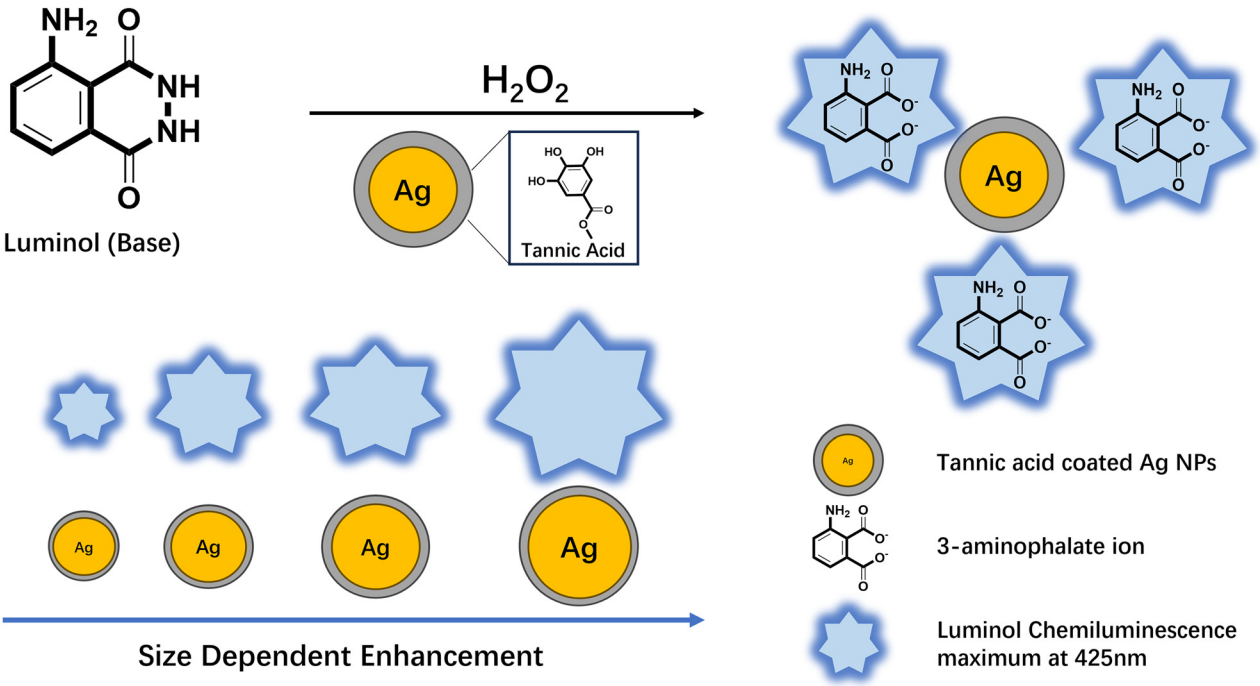

Fig. 1 Schematics of the luminol chemiluminescence reaction. Luminol, in its basic form, undergoes oxidation by H_2O_2, leading to the formation of an unstable intermediate state known as 3-aminophthalate, which subsequently decays to emit photons. With the plasmonic coupling (TA–Ag NPs) introduced, the decay of the excited luminescence molecules is facilitated. As a result, the chemiluminescence is magnified. The luminol molecules are adsorbed to Ag NPs by the tannic acid spacer layer. The enhancement is size-dependent, with the bigger-sized NPs introducing a higher enhancement.

We introduced tannic acid-coated functionalised plasmonic Ag nanospheres into luminol chemiluminescence reactions to systematically investigate the factors influencing PEC enhancement, as illustrated in Fig. 1. We sequentially explored three key factors: the optimal size of Ag nanoparticles, the most effective surface functional group, and the concentration of nanoparticles. By integrating these insights, we engineered enhanced plasmonic nanostructures tailored to maximise chemiluminescence enhancement. Significantly, we deconvoluted the enhancement pathways including the catalytic enhancement and plasmonic induced enhancement. Our study achieves over two orders of magnitude PEC enhancement, offering significant potential to advance practical applications such as improving the detection limits of chemiluminescence-based biosensors. These findings, coupled with the innovations introduced, including the utilisation of tannic acid-coated Ag nanospheres and the systematic examination of influencing factors, pave the way to substantial progress in the fields of analytical chemistry, forensic science, and interdisciplinary research in biology and chemistry.

Materials and methods

Reagents and materials

Silver nitrate ($AgNO_3$), tannic acid (TA), trisodium citrate dihydrate (TSC), luminol, hydrogen peroxide solution (50 wt% H_2O_2), sodium hydroxide (NaOH), sodium carbonate (Na_2CO_3), sodium bicarbonate ($NaHCO_3$) was purchased from Sigma-Aldrich, UK. Hydrochloric acid (HCl, 37%), nitric acid (HNO_3, 68%) and ethanol were obtained from VWR International, UK. De-ionized (DI) water purified using the Millipore Mili-Q gradient system (>18.2 MΩ) was used for all the procedures. All glassware was cleaned using Aqua Regia and rinsed with ethanol and DI water.

A 1.0×10^{-2} mol L^{-1} stock solution of luminol was prepared by dissolving 0.1772 g of luminol in 100 ml of 0.1 mol L^{-1} NaOH solution. Working solutions of luminol (1.0×10^{-4} mol L^{-1}) were diluted by the carbonate buffer (pH = 9.32). The working H_2O_2 solutions at 0.15 mol L^{-1} were prepared daily from the 50 wt% H_2O_2 stock solution.

Synthesis of Ag nanoparticles

TA functionalised Ag nanospheres (Ag NPs) of four different sizes were synthesised by following the method published by N. G. Bastús *et al.* to realise the formation of highly monodispersed Ag NPs.[18] The four sizes are referred to as TA–Ag 31, TA–Ag 41, TA–Ag 53 and TA–Ag 93. TA represents the surfactant group (tannic acid) on Ag NPs, and the numbers represent the diameters of the Ag cores with the unit in nm. Briefly, a 100 ml aqueous mixture of TSC (5 mM) and TA (2.5 mM) was heated in a silicon oil bath with a condenser for 15 minutes under vigorous stirring until boiling. Then, 1 ml of $AgNO_3$ (25 mM) was rapidly injected into the boiling solution to form the Ag seeds. The heating temperature was set to 90 °C followed by injecting 500 μl of TSC (25 mM), 1.5 ml of TA (2.5 mM) and 1 ml of $AgNO_3$ (25 mM). After reacting for 30 minutes, 40 ml of Ag solution was extracted, and the mixture was diluted with 37 ml DI water. The injection and dilution procedures were repeated

3 times to get TA–Ag 31–93 solutions. Different generations of Ag NPs were synthesised in this method by growing nanoparticles based on the previous generation of TA–Ag NPs. The tannic acid worked as a weak reducing agent and a capping agent to limit the further growth of Ag NPs. Finally, TA–Ag NPs solutions were centrifuged at 6000 rpm for 1 hour to wash off the excess TA and TSC.

Instrumentation

As-prepared TA–Ag NPs were characterised by an Agilent Cary 5000 UV-VIS-NIR spectrophotometer. The surface resonance wavelengths of the nanoparticles were determined from the absorbance spectra. Transmission electron microscopy (TEM) was performed in a JEOL JEM-2100F with an accelerating voltage of 200 kV. The images of Ag NPs were processed by ImageJ software to calculate the size distributions of the TA–Ag NPs.

Inductively coupled plasma optical emission spectroscopy (ICP-OES) was applied to measure the Ag ion concentrations. The samples were centrifuged at the same speed and resolved in 27.5% HNO_3. A set of standard solutions with known concentrations was measured to generate a calibration curve as shown in Fig. S1 (ESI†). The signal from the samples were then detected and compared with the calibration curve to calculate the concentration of Ag samples.

The number density of the NPs was calculated from the ion concentrations based on the volume of the NPs (approximate the NPs into sphere) and the density of Ag metal (1.049×10^{-17} mg nm^{-3}). As shown in Table S1 (ESI†), the number density of Ag NPs is calculated by dividing the total mass (ppm) with the mass of one Ag NP. The Table S2 (ESI†) then used the surface area of one Ag nanosphere and the number density of Ag NPs from Table S2 (ESI†) to calculate the total surface area of different TA–Ag NPs.

Results and discussion

Tannic acid (TA) functionalised Ag NPs were prepared by a citrate reduction method with the aid of tannic acid as the stabiliser.[18] The Ag NPs synthesised by this method were highly monodispersed and had a narrow size distribution, as indicated in Fig. 2a–d. Four different sizes of tannic acid coated Ag NPs were synthesised referred to as TA–Ag 31, TA–Ag 41, TA–Ag 53 and TA–Ag 93.

The optical extinction spectra of TA–Ag NPs showed plasmonic peaks between 400 and 500 nm, shown in Fig. 2e. In luminol chemiluminescence reactions, the chemiluminescence peak is centred at 425 nm when the excited state formed is 3-aminophthalate.[19] The overlap between the plasmonic peak of Ag and the chemiluminescence peak of luminol is one of the key requirements for plasmonic-enhanced chemiluminescence to take place.[20]

The quenching effect is an unwanted energy transfer from excited state energy to the electrons in metal surface during the chemiluminescence reaction, resulting in a reduction in chemiluminescence intensity.[21] Quenching only occurs when the emitters have direct contact with the plasmonic nanoparticle

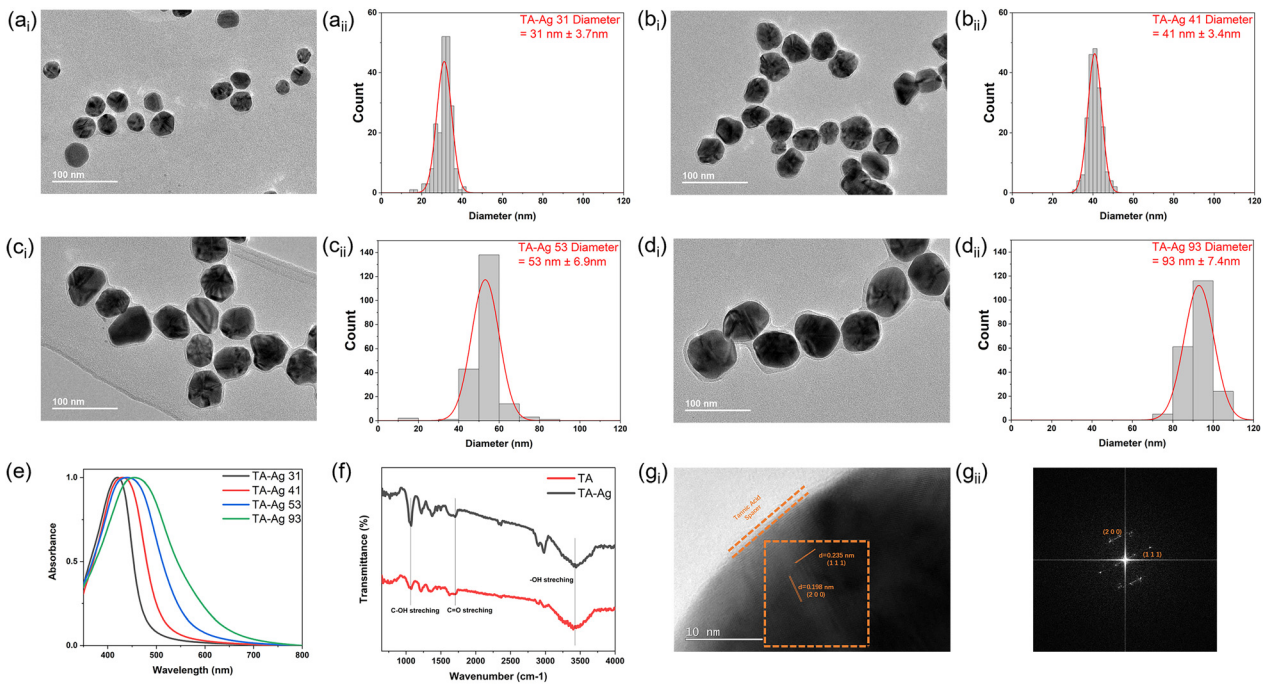

Fig. 2 (a)–(d) TEM images and size distributions depicting four sizes of Ag nanospheres. The NPs were synthesised by reducing $AgNO_3$ using a boiling mixture of TA and TSA. The size distribution graphs illustrate the increase in Ag NPs size, ranging from 31, 41, 53 to 93 nm. (e) Absorbance spectra of Ag NPs with varying sizes. A clear red shift is observed, accompanied by a broader distribution, as the size of Ag NPs increases. The shift results in a larger overlap area with luminol chemiluminescence. (f) The FTIR plot confirming the presence of the spacer layer as tannic acid. (g) High-resolution TEM image showcasing the detailed structure of Ag NPs.

surface.[22–24] Therefore, a spacer layer that isolates the emitters from the plasmonic nanoparticle surface is crucial to realise enhancement.[25] In this study, the synthesised Ag NPs exhibited a naturally occurring spacer layer, as illustrated in Fig. 2g. The composition of this spacer layer was characterised *via* FTIR analysis. As indicated in Fig. 2f, the spectrum verified that the spacer layer was composed of tannic acid, a polyphenol renowned for its nanoparticle-stabilizing attributes. Unlike the commonly used silica as a spacer material, the potential for enhancing chemiluminescence performance with Ag NPs by employing tannic acid (TA) as the spacer layer remains uncharted. From the synthesis procedure perspective, silica coating requires a precise control over the ethanol to water ratio, tetraethyl orthosilicate (TEOS) and ammonia solution concentration, in combination with the total surface area of Ag NPs to get a silica layer of target thickness (5–15 nm).[26] In contrast, TA is a spacer formed on Ag NPs surfaces and does not require further treatments. In the following experiments, it is proved that TA spacer layers can efficiently reduce the quenching effect while retaining the plasmonic properties of Ag NPs.

The interaction between TA coated nanoparticles and luminol was investigated by mixing Ag NPs with a luminol working solution and H_2O_2 in a transparent cuvette. The chemiluminescence spectra of pure luminol and that after the addition of TA–Ag NPs were recorded (Fig. 3a inset). The concentrations of TA–Ag 31 to 93 were measured by ICP to ensure that the same number of Ag NPs were used in the different tests. Since the luminol chemiluminescence intensity decays over time, the spectra of all the reactions were compared at the same time point.

Compared to the pure luminol reaction, which exhibited low intensity, the addition of TA–Ag NPs resulted in a significant enhancement of the chemiluminescence signal. The enhancement factors increased with the increasing size of TA–Ag NPs, as indicated in Fig. 3a. Significantly, the incorporation of TA–Ag 93 into the luminol–H_2O_2 reaction showed a maximum enhancement of up to 175-fold. The observed chemiluminescence enhancement of TA–Ag nanoparticles on luminol is due to the near-field interactions of the chemically induced excited states of luminol with resonant surface plasmons in Ag nanoparticles. It has been reported that the enhanced chemiluminescence depends on the spectral overlap between the LSPR in the metal nanostructures with the optical properties of the chemiluminescent species.[27] Therefore, by maximizing the overlap of the absorption/emission spectra of luminol with the LSPR of Ag nanoparticles, the maximum chemiluminescence enhancement is expected. In our case, there is a significant overlap between the plasmonic response of Ag nanoparticles and the chemiluminescence spectrum of the luminol, which could explain this dramatic enhancement.

Luminol chemiluminescence reaction is a flash-type luminescence that has a short stability window at maximum intensities.[28] In this study, the effect of plasmonic Ag nanoparticles on stability was determined over a period of 20 minutes (Fig. 3b). The TA–Ag 93 enhanced chemiluminescence reaction has both higher intensities and stability than the pure luminol reaction within the 20-minute period, indicating plasmonic Ag nanoparticles not only enhancing the chemiluminescence intensity but also increase chemiluminescence time.

In contrast to previous studies,[15] it was observed that as the nanoparticle size increases, the enhancement factors of chemiluminescence increase (Fig. 3a). To gain deeper insights, chemiluminescence performance assessments were conducted using commercially available silver nanoparticles (Ag NPs) stabilised with citrate acid. The same number of CIT-Ag NPs was incorporated into the luminol chemiluminescence reactions. To compare with TA–Ag NPs, the same amount of luminol and H_2O_2 were used. As shown in Fig. 4a, our observations align with the existing literature about the catalytic effect, *i.e.*, the smaller the NPs the greater the chemiluminescence enhancement. The smaller NPs possess higher surface-to-volume ratios to impart superior catalytic properties. Therefore, CIT-Ag with 10 nm diameter had the best performance. Notably, when the nanoparticle size reaches 100 nm, the catalytic enhancement becomes nearly negligible. Thus, suggesting that the 175-fold enhancement by

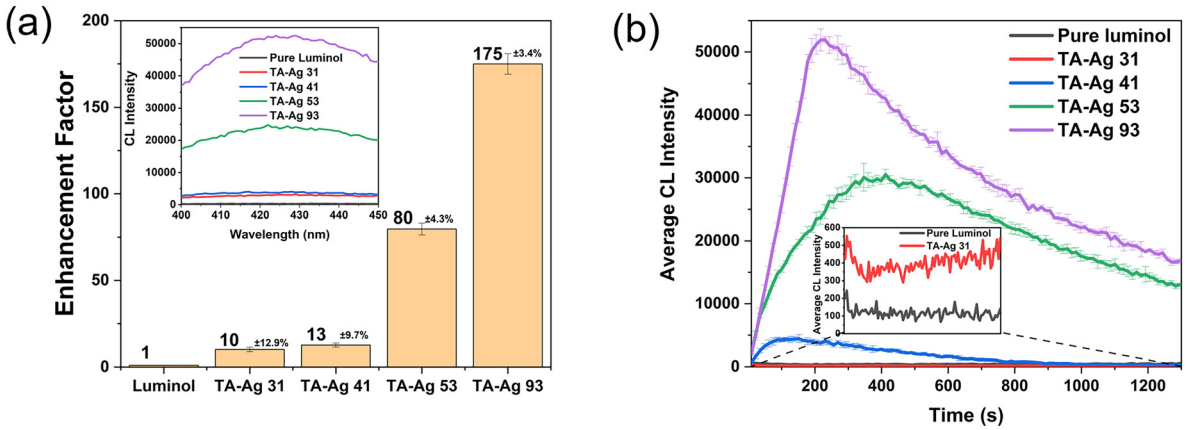

Fig. 3 (a) The chemiluminescence spectra of luminol–H_2O_2 reactions with and without the incorporation of TA–Ag 31–93 nm. In the pure luminol reaction, a peak at around 425 nm is observed. The addition of TA–Ag NPs does not alter the chemiluminescence peak position. The introduction of TA–Ag NPs leads to enhancements of 10, 13, 80 and 175-fold respectively. (b) Stability of luminol chemiluminescence intensity over time, with intensities measured at 425 nm every 13 seconds. TA–Ag 93 elongates the stability of luminol chemiluminescence reactions.

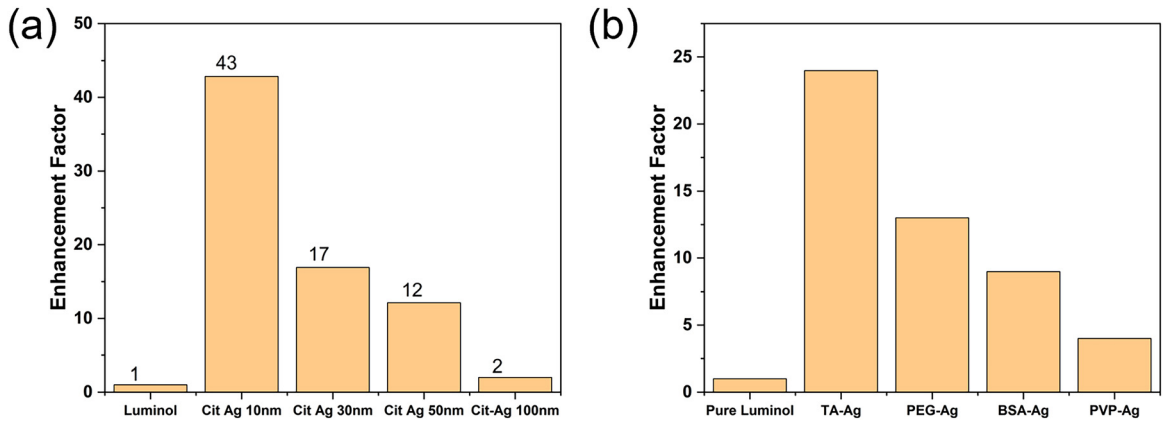

Fig. 4 (a) The catalytic effect increases with the decreasing NP size. When the NP reaches 100 nm, the catalytic effect is almost negligible. This proves the plasmonic-dominated enhancement in the TA–Ag enhanced luminol chemiluminescence reaction. (b) The comparison of the chemiluminescence performance of Ag NPs capped with different spacers. TA–Ag exhibits the most significant plasmonic enhancement effect due to hydrogen bonds forming between TA and luminol.

TA–Ag 93 is mainly contributed to by the plasmonic properties of Ag NPs.

Due to the strong increase in the intensity of the chemiluminescence, compared to previously reported enhancement factors, the impact of various spacers was also investigated. The spacer layers we studied included bovine serum albumin (BSA), polyvinylpyrrolidone (PVP), polyethylene glycol (PEG), and tannic acid (TA). The interactions between luminol molecules and Ag NPs were investigated. Despite the neutral charge nature of these spacers, we observed distinct responses of luminol molecules in proximity to Ag NPs, with TA demonstrating the most pronounced enhancement, as illustrated in Fig. 4b.

The amino group in luminol molecules could form hydrogen bonds with the hydroxyl groups in TA–Ag, ensuring that each Ag NP effectively attracts luminol molecules.[29] In contrast, other spacers, lacking functional groups, do not have a mechanism to guarantee the proximity of luminol molecules to the plasmonic Ag nanoparticles, resulting in weak plasmonic enhancement and mainly catalytic enhancement in chemiluminescence measurements. The TA spacer also plays a crucial role in maintaining the appropriate separation distance between Ag NPs and luminol molecules, thereby facilitating the plasmonic enhancement, which is a localised effect.

The influence of separation distance on chemiluminescence enhancement was further explored by fabricating silica spacers of varying thicknesses. Silica spacers effectively prevent ion diffusion to NPs, thus exclude catalytic effects. Notably, when the spacer thickness exceeded a certain threshold, it was observed to have a dampening effect on the plasmonic properties of Ag NPs, leading to the quenching of luminol chemiluminescence (Fig. S2, ESI†). This finding underscores the delicate balance required in spacer design to achieve optimal plasmonic enhancement while avoiding quenching effects due to excessive separation distances.

Moreover, we investigated the catalytic property of TA–Ag 93 by applying the nanoparticles in luminol–$AgNO_3$ chemiluminescence reaction. It has been reported that the oxidation of luminol by $AgNO_3$ is strongly catalysed by Ag nanoparticles.[30] However, the absence of discernible chemiluminescence intensity as recorded here by the measuring instrument (Fig. S3, ESI†) indicates that TA–Ag 93 NPs did not catalyse the chemiluminescence reactions.

In another chemiluminescence test the total surface area of the 4 different sized TA–Ag NPs was kept constant, the results demonstrated that the plasmonic enhancement trend remained almost unaffected by this factor (Fig. S4, ESI†). Still, TA–Ag 93 emerges as a favoured choice of particle size, facilitating the attainment of the most significant plasmonic enhancement.

Finite-difference time-domain (FDTD) modelling was applied to gain a deeper understanding of the optical properties of Ag nanoparticles. The primary focus of this modelling was to characterise the extinction cross-section and analyse the ratios of absorption and scattering cross-section for all the four different sizes of Ag nanoparticles studied. A simulation geometry was firstly created, followed by setting incident light wavelength, polarisation and direction, to generate extinction spectra. The spectra tracked the interaction between incident light with the different nanoparticles, showing the absorption and scattering cross-sections, which increased with particle size as shown in Fig. 5a–d. However, when the nanoparticle size reached a critical threshold of 53 nm in Fig. 5c, it was observed that the scattering cross-section began to outweigh the absorption cross-section. The simulated results are consistent with experimental results conducted by D.D. Evanoff *et al.*[31]

In a chemiluminescence reaction, chemically excited molecules are unstable and prone to relax to the ground state. The total relaxation rate is the sum of radiative and non-radiative decay, while only the radiative decay releases photons. With the incorporation of plasmonic Ag nanoparticles in the chemiluminescence reaction, the relaxation rate is substantially boosted. Studies show that when the excited molecules to nanoparticle distance is smaller than 4 nm, non-radiative decay increases.[32,33] In this study, the thickness of TA spacers is more than 4 nm, which ensures the separation distance is long enough to maintain the non-radiative decay at the same level after plasmonic

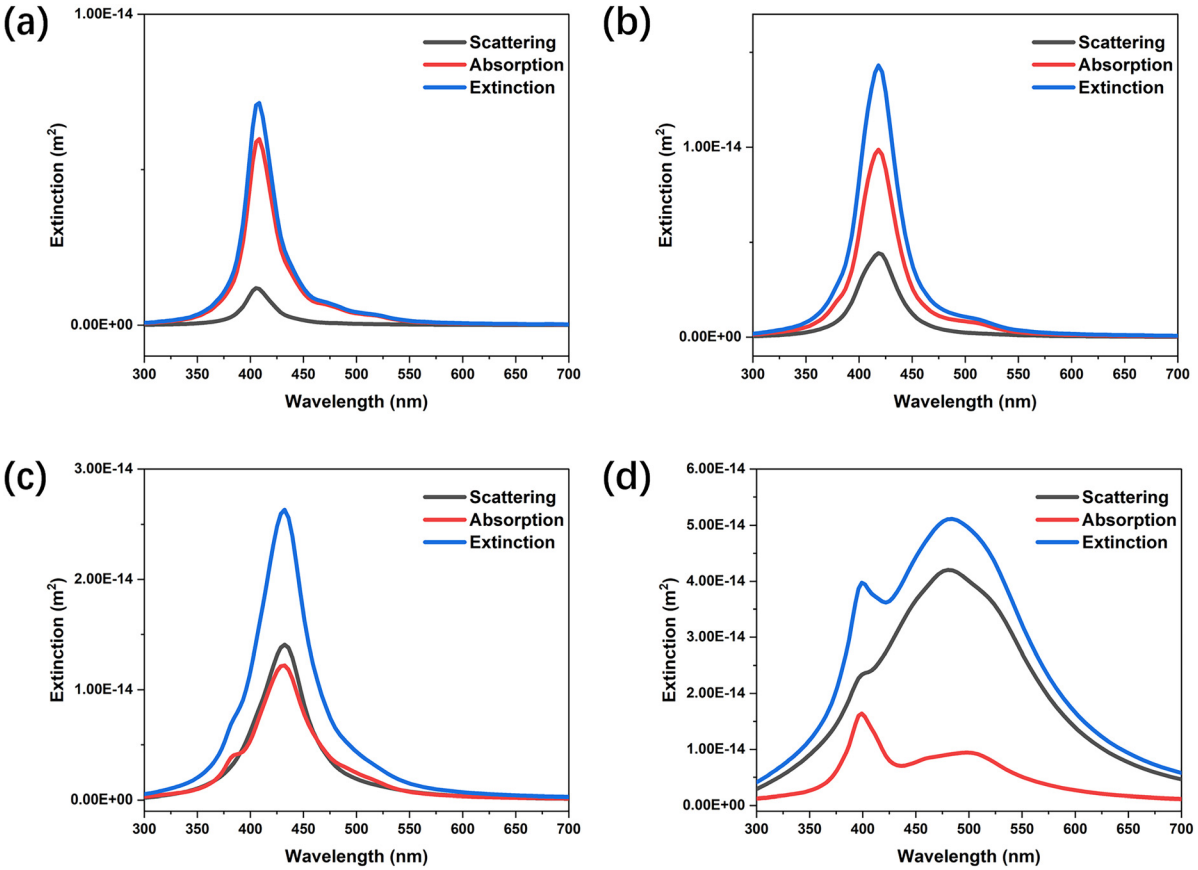

Fig. 5 (a)–(d) The extinction cross-sections of TA–Ag 31, 41, 53, 93 modelled by FDTD. The scattering cross-sections overtake the absorption cross-section as the sizes increase to 53 nm.

coupling. Benefiting from the increasing scattering cross-section, bigger TA–Ag NPs increase the far-field coupling efficiency and accelerate the radiative decay, leading to the emission enhancement.[34] This enhancement could be attributed to the overlapping between the scattering spectrum of plasmonic nanoparticles with the chemiluminescence emission spectrum. Thereby, the significant 175-fold enhancement in luminol chemiluminescence intensity achieved by TA–Ag 93 NPs incorporation was due to the dominant scattering cross-section of the nanoparticles, validating the significance of scattering in plasmonic enhanced chemiluminescence.

In addition to the factors previously discussed, the concentration of TA–Ag NPs plays a significant role in influencing the chemiluminescence enhancement factors. Our investigation included an examination of the correlation between transmittance and chemiluminescence enhancement, as shown in Fig. 6a. The original TA–Ag 93 solution, with a particle density of 3.8×10^8 NPs ml^{-1}, underwent various adjustments through dilution with buffer solutions or concentration *via* centrifugation and redispersion. At higher concentrations (1.9×10^9 and 3.8×10^9 NPs ml^{-1}), the solution displayed self-absorption of the blue light emitted during the luminol chemiluminescence reaction. Chemiluminescence enhancement exhibited an initial increase at lower TA–Ag 93 solution concentrations, reaching a plateau of 4.75×10^8 NPs ml^{-1}. Further dilution resulted in decreased enhancement due to there being an insufficient number of plasmonic TA–Ag 93 nanoparticles available to facilitate photon emissions. Thus, optimising Ag nanopaticle concentration plays a pivotal role in controlling and enhancing luminol chemiluminescence reactions.

To further explore the potential application of TA–Ag nanoparticles, TA–Ag 93 were introduced into the reaction between Fe^{3+}–luminol–H_2O_2, aiming to enhance the chemiluminescence intensity of the reaction. Different to luminol–H_2O_2 reaction in the previous sections with relatively high solution concentrations, the chemiluminescence reaction in this test takes place with slower kinetics so that it does not illuminate at low luminol–H_2O_2 concentrations. However, it has been proved that Fe ions are able to catalyse the luminol–H_2O_2 reaction and emit visible blue light.[35] Fe is one of the transition metals that is able to catalyse the luminol chemiluminescence reaction. The oxidation state of Fe ions switches between the ferrous and ferric states in H_2O_2 and accelerates its decomposition, forming radicals to react with luminol.[36] The normal Fe ion level in adults' blood is 10–32 μmol L^{-1}.[37] Therefore, in a crime scene, low concentration luminol–H_2O_2 is used to visualise the traces of blood since only the area with Fe ions can trigger the chemiluminescence reaction and emit blue light.

In the experimental setup, six distinct Fe ion concentration solutions were prepared, ranging from 32 μmol L^{-1} down to

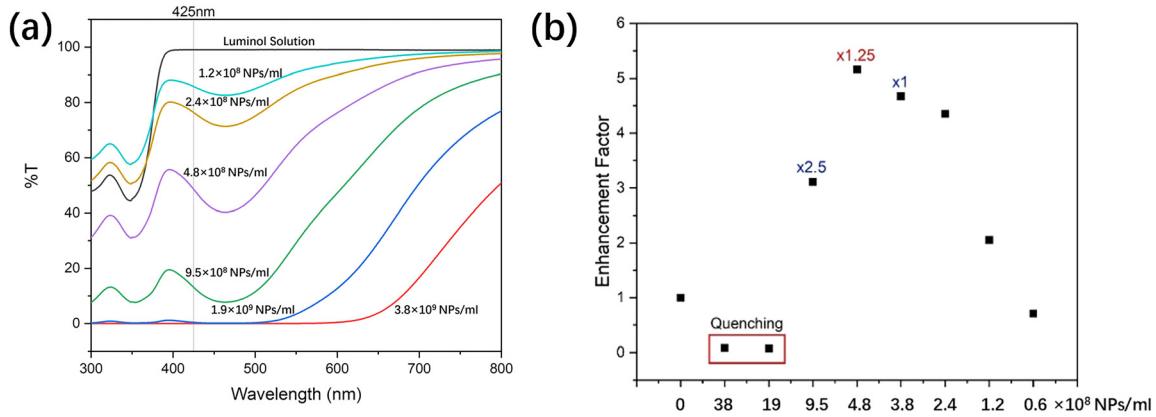

Fig. 6 (a) Light transmittance spectra of varying concentrations of TA–Ag 93 solutions. As the NPs solutions become more concentrated, the transmittance of blue light decreases, resulting in self-absorption and reduced emission intensity. (b) CL intensity spectra of luminol CL reactions enhanced by different concentrations of TA–Ag 93 solutions. The optimised concentration is x1.25 times more concentrated TA–Ag 93 solutions.

5 μmol L^{-1}, encompassing the concentrations within and below the typical range found in an adult's blood.[37] Each Fe ion solution was dropped and dried uniformly to 6 filter papers with plastic backs for experimentation (two sets of parallel tests were set up). Two mixtures of luminol and H_2O_2 solutions were prepared, with one mixture containing TA–Ag 93 nanoparticles while the other contained an equivalent volume of water. Subsequently, both mixtures were applied simultaneously to the two sets of filter papers to compare the chemiluminescence performance with and without TA–Ag 93 nanoparticles. The light intensity should be related to the concentration of Fe ions. Photographs were taken 60 seconds after the reaction commenced and the chemiluminescence intensity was quantitatively analysed using ImageJ.[38]

As shown in Fig. 7, the calibration curves for Fe ion quantification show that the plasmonic enhanced chemiluminescence by the TA–Ag 93 nanoparticles, led to a lower detection limit (the background intensity is 3.5 ± 1 RLUs) and a broad dynamic range for the detection of Fe ion. When there are no TA–Ag NPs incorporated (black dots), the chemiluminescence intensity proportionally increases with Fe ion concentration. However, the chemiluminescence intensity below 10 μmol L^{-1} is too low to be detected (the intensity is lower than 8.5 RLUs). The signal is also weak at higher Fe ion concentrations. As the normal Fe ion level for adults is 10–32 μmol L^{-1}, the conventional luminol–H_2O_2 reaction alone lacks the sensitivity to diagnose anaemia conditions accurately. But with the incorporation of plasmonic TA–Ag 93 nanoparticles (Red dots), the signal is significantly magnified. The sensitivity is also greatly improved, extending below 10 μmol L^{-1} and reaching the detection limit of 0.5 μmol L^{-1}. Remarkably, this method requires only a minimal blood volume of 20 μl, significantly less than that of the standard blood tests. Thus, it offers a rapid, convenient, and precise testing approach.

Fig. 7 illustrates that plasmonic TA–Ag 93 nanoparticles possess the capability to significantly amplify the light intensity resulting from the Fe^{3+}–luminol–H_2O_2 reaction. Our innovative approach allows for the detection of even minute traces of

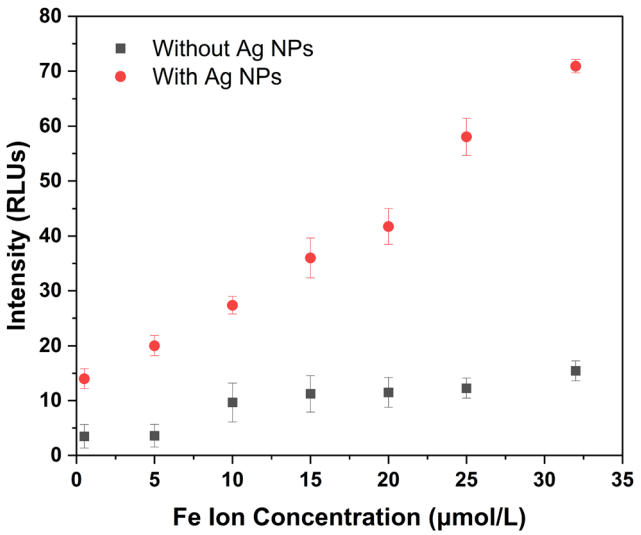

Fig. 7 Calibration curves for Fe ion concentration with and without the incorporation of TA–Ag 93 NPs. The normal Fe ion level for adults is 10–32 μ mol L^{-1} of blood. Without TA–Ag 93 NPs, the luminol–H_2O_2 system exhibits weak luminescence. The introduction of TA–Ag 93 NPs reduced the limit of detection and enhanced the intensity at higher concentrations, facilitating clearer observations.

blood with high reliability. This breakthrough enhances the probability of uncovering critical evidence that might otherwise remain concealed, thus contributing substantially to the resolution of forensic evidence.

Conclusions

This work successfully harnessed the remarkable enhancement capability of tannic acid coated Ag nanoparticles in luminol–H_2O_2 chemiluminescence reactions. The significant enhancement factor is up to 175-fold for TA–Ag 93. With FDTD modelling and experimental investigation, we found out the main pathway for the enhancement is due to the plasmonic effect, which in turn, is controlled by plasmonic nanoparticle sizes,

spacer layers and nanoparticle densities. We also demonstrated our plasmonic platform enables sensitive Fe ion detection with a microlitre volume of samples. The promising results demonstrated in this work pave the way for its practical applications in forensic science, *in vitro* diagnosis, and research in biology and chemistry.

Author contributions

Y. L. conducted experiments and advanced characterisations, including Ag nanoparticles synthesis, plasmonic enhanced chemiluminescence investigation. J. X and Y. L designed and carried out Fe ion level concentration test. D. J. R and F. X, supervised the project. F. X. conceptualised and planned the research. All authors read and commented on the paper.

Conflicts of interest

There are no conflicts to declare.

Acknowledgements

The authors acknowledge and use of characterisation facilities within the Harvey Flower Electron Microscopy Suite at the Department of Materials, Imperial College London. The authors acknowledge Prof. Rupert Oulton for providing the license of Ansys Lumerical Mie scattering (FDTD).

References

1 F. Barni, S. W. Lewis, A. Berti, G. M. Miskelly and G. Lago, *Talanta*, 2007, **72**, 896–913.
2 T. Takayanagi, Y. Inaba, H. Kanzaki, Y. Jyoichi and S. Motomizu, *Talanta*, 2009, **79**, 1089–1093.
3 F. Patolsky, E. Katz and I. Willner, *Angew. Chem., Int. Ed.*, 2002, **41**, 3398–3402.
4 T. Nagy-Simon, A.-M. Hada, S. Suarasan and M. Potara, *J. Mol. Struct.*, 2021, **1246**, 131178.
5 D. R. Dadadzhanov, I. A. Gladskikh, M. A. Baranov, T. A. Vartanyan and A. Karabchevsky, *Sens. Actuators, B*, 2021, **333**, 129453.
6 A. M. García-Campaña and W. R. G. Baeyens, *Analusis*, 2000, **28**, 686–698.
7 C. Lu, G. Song and J.-M. Lin, *TrAC-Trend Anal. Chem.*, 2006, **25**, 985–995.
8 G. Barbillon, *Materials*, 2019, **12**, 1502.
9 W. Hergert and T. Wriedt, *The Mie theory: basics and applications*, Springer, 2012.
10 G. A. Mansoori, *UN-APCTT Tech Monitor*, 2002, **19**, 53–59.
11 S. M. Fothergill, C. Joyce and F. Xie, *Nanoscale*, 2018, **10**, 20914–20929.
12 J. Xu, W. Morton, D. Jones, T. A. Tabish, M. P. Ryan and F. Xie, *Appl. Phys. Rev.*, 2022, **9**, 031406.
13 J. S. Pang, I. G. Theodorou, A. Centeno, P. K. Petrov, N. M. Alford, M. P. Ryan and F. Xie, *ACS Appl. Mater. Interfaces*, 2019, **11**, 23083–23092.
14 M. H. Chowdhury, K. Aslan, S. N. Malyn, J. R. Lakowicz and C. D. Geddes, *J. Fluoresc.*, 2006, **16**, 295–299.
15 H. Chen, F. Gao, R. He and D. Cui, *J. Colloid Interface Sci.*, 2007, **315**, 158–163.
16 M. H. Chowdhury, K. Aslan, S. N. Malyn, J. R. Lakowicz and C. D. Geddes, *Appl. Phys. Lett.*, 2006, **88**, 173104.
17 Z. Zhang, H. Cui, C. Lai and L. Liu, *Anal. Chem.*, 2005, **77**, 3324–3329.
18 N. G. Bastús, F. Merkoçi, J. Piella and V. Puntes, *Chem. Mater.*, 2014, **26**, 2836–2846.
19 L. Wang, P. Yang, Y. Li, H. Chen, M. Li and F. Luo, *Talanta*, 2007, **72**, 1066–1072.
20 A. Kannegulla, Y. Liu, B. Wu and L.-J. Cheng, *J. Phys. Chem. C*, 2018, **122**, 770–776.
21 J. R. Lakowicz, *Principles of fluorescence spectroscopy*, Springer, 2006.
22 W. Yin, J. Sui, G. Cao and D. Dabiri, *Talanta*, 2023, **259**, 123690.
23 G. Yang, Y. Liu, Y. Hui, T. Jisi, D. Chen, D. A. Weitz and C. X. Zhao, *Angew. Chem., Int. Ed.*, 2021, **60**, 15426–15435.
24 F. Meng, J. Wang, Q. Ping and Y. Yeo, *ACS Nano*, 2018, **12**, 6458–6468.
25 J.-H. Choi, J. Lim, M. Shin, S.-H. Paek and J.-W. Choi, *Nano Lett.*, 2021, **21**, 693–699.
26 Y. Hu, Y. Shi, H. Jiang, G. Huang and C. Li, *ACS Appl. Mater. Interfaces*, 2013, **5**, 10643–10649.
27 K. Aslan and C. D. Geddes, *Chem. Soc. Rev.*, 2009, **38**, 2556.
28 A. Karabchevsky, A. Mosayyebi and A. V. Kavokin, *Light: Sci. Appl.*, 2016, **5**, e16164.
29 A. Baldwin and B. W. Booth, *J. Biomater. Appl.*, 2022, **36**, 1503–1523.
30 S. Li, H. Sun, D. Wang, J. Hong, S. Tao, H. Yu, X. Wang and X. Wei, *Luminescence*, 2012, **27**, 211–216.
31 D. D. Evanoff and G. Chumanov, *J. Phys. Chem. B*, 2004, **108**, 13957–13962.
32 D. H. Waldeck, A. P. Alivisatos and C. B. Harris, *Surf. Sci.*, 1985, **158**, 103–125.
33 T. Soller, M. Ringler, M. Wunderlich, T. A. Klar, J. Feldmann, H. P. Josel, Y. Markert, A. Nichtl and K. Kürzinger, *Nano Lett.*, 2007, **7**, 1941–1946.
34 R. Bardhan, N. K. Grady, J. R. Cole, A. Joshi and N. J. Halas, *ACS Nano*, 2009, **3**, 744–752.
35 T. D. W. Andrew and L. Rose, *Anal. Chem.*, 2001, **73**, 5909–5920.
36 C. Plieth, *ACS Omega*, 2019, **4**, 3268–3279.
37 M. Munoz, J. A. Garcia-Erce and A. F. Remacha, *J. Clin. Pathol.*, 2011, **64**, 287–296.
38 C. A. Schneider, W. S. Rasband and K. W. Eliceiri, *Nat. Methods*, 2012, **9**, 671–675.

